Pulsed CO_2 Laser-Induced Effects on Water Droplets

M. Autric,* P. Vigliano,† D. Dufresne,‡ J. P. Caressa,§ and Ph. Bournot‡
Institute of Fluid Mechanics, CNRS, Marseilles, France

Pulsed high-power CO_2 laser beams propagating through the atmosphere can be affected by such different linear or nonlinear phenomena as aerosol and molecular absorption, scattering, turbulence, thermal blooming, or optical breakdown, depending on the atmospheric characteristics and laser parameters. An experimental investigation was carried out to study the pulsed CO_2 laser-induced effects on water droplets. Water droplets with radii of 8–400 μm were irradiated. The average fluences used for the interaction were between 1 and 4 J/cm^2 (1.6–6.4 J/cm^2 on the droplet) for a pulse duration adjustable between 2 and 6 μs. Most measurements were made using an Imacon 790 converter camera allowing framing rates of between 10^4 and 2×10^7 frames/s with fast framing and a scanning rate of between 1 ns/mm and 1 μs/mm with streak photography. The experimental results presented in this paper identify four main mechanisms that can occur sequentially throughout the laser interaction, without specifying which dominate over the others: vaporization, deformation, shattering, and propulsion. In particular, with time, evolution of the hot vapor and shock wave produced by the vaporization of a single water droplet was observed. Evolutions of the droplet deformation with time is shown. Threshold values and characteristic shattering times of the liquid particles are given, as well as the drop velocities and ejection directions across the area illuminated by the laser pulse.

Nomenclature

c	= velocity of sound
C_p	= specific heat
E	= laser energy
F	= laser fluence absorbed by the droplet
I	= mechanical impulse
l_v	= latent heat of vaporization
L_{abs}	= absorption length, $\simeq 10$ μm
L_v	= $C_p \Delta T + l_v \simeq 2.6$ KJ/g
m	= mass flux of the vaporized water
P_e	= average effective overpressure
$Q_A(R)$	= Mie absorption coefficient
r	= shock wave position
R	= radius of the droplet
R_f	= final droplet radius
R_0	= initial droplet radius
T	= temperature
U	= speed of the center of mass
v	= blast wave velocity
γ	= ratio of specific heat
ν	= kinematic viscosity of water
ρ	= water density
ρ_0	= air density
σ	= coefficient of surface tension, ~ 75 dyne/cm for water
ϕ	= incident laser intensity

Introduction

PROPAGATION of high-energy laser beams through the atmosphere is greatly disturbed due to the breakdown induced by aerosols.[1–6] In fact, optical breakdown leads to the formation of an expanding plasma that absorbs much of the incident laser radiation. In pure air, this phenomenon arises when the laser intensity is greater than a threshold value on the order of 3×10^9 W/cm^2. Aerosols in suspension in the atmosphere lower the local breakdown threshold values, which thus depend essentially on the aerosol dimensions. Experimental studies[1] have shown a relationship of D^{-1} for $D < 10$ μm and $D^{-0.07}$ for $D > 10$ μm, where D is the average diameter of the aerosols. Consequently, by modifying the aerosol granulometric distribution along the beam path, it would seem to be possible to increase the transmission of light energy. Experiments made in and out of the laboratory using a precursor pulse have shown the existence of an atmospheric "clearing" effect.[7–12] This effect is characterized by an increase in the breakdown threshold and in the energy transmission of the second pulse. Thus, knowledge of the thermomechanical mechanisms occuring when a laser beam interacts with a water droplet is important in order to maximize the propagation of high-intensity laser pulses, especially for atmospheric conditions such as haze, fog, or clouds in which airborne particle concentrations are particularly high and for rain in which the water drops are large.

Previously published experiments[13,14] described the explosive vaporization and shattering of water droplets upon irradiation with a submicrosecond pulse from a 10.6 μm laser. These works clearly showed front surface heating (droplet radius > 15 μm) and volume heating (droplet radius < absorption length). More recent results have described and compared all of these mechanisms at lower intensities with larger droplets.[4–15]

An experimental investigation was carried out to study the pulsed CO_2 laser-induced effects on water droplets with radii of 8–400 μm. The average fluences were 1–4 J/cm^2 for an adjustable pulse duration of 2–6 μs (i.e., intensities of 10^5–10^6 W/cm^2).

The experimental study presented here identifies the four main mechanisms occurring sequentially throughout the interaction: vaporization, deformation, shattering, and propulsion of the droplet out of the focal volume. In particular, the evolution with time of the hot vapor and of the shock wave produced by the vaporization of a single droplet was observed.

Presented as Paper 85-1630 at the AIAA 18th Fluid Dynamics, Plasmadynamics and Lasers Conference, Cincinnati, OH, July 16–18, 1985; received Sept. 18, 1985; revision received March 31, 1987.

*Research Scientist, Laser-Matter Interaction Group. Member AIAA.

†Maître-Assistant, Université de Toulon et du Var, also working with the Laser-Matter Interaction Group.

‡Maître de Conférences, Université d'Aix-Marseille, also working with the Laser-Matter Interaction Group.

§Research Scientist, Laser-Matter Interaction Group (presently with Laboratoire d'Aérothermique du CNRS, Meudon, France).

The evolution with the time of droplet deformation is shown. Threshold values and characteristic shattering times of the liquid particles are given. Drop velocities and ejection directions across the area illuminated by the laser pulse are also presented.

Experimental Equipment

The experimental apparatus is shown in Fig. 1. Water droplets of radii between 30 and 400 μm were produced using a classical atomizer and were suspended using spiderwebs (thread diameter ≤ 10 μm). A liquid aerosol generator developed at Laboratoire d'Aerothermique de Meudon[16] was also used to produce droplets of 8–30 μm radius. Therefore, no support was used to hold them, their dimensions being too small. The drops were exposed to radiation from a cold-cathode electron CO_2 laser gun able to deliver up to 1000 J for a pulse time of 2–6 μs. Pulses consisted of an initial high-power gain-switched spike (80 ns FWHM) followed by a high-energy tail. (The ratio of peak power to tail power is about 3 or 4).

An unstable optical resonator (equivalent Fresnel number = 20) produced an annular-shaped beam (external diam 150 mm, internal diam 100 mm).

The average fluences used for the interaction were between 1 and 4 J/cm^2. The spatial intensity profile across the beam was measured using a $LiTaO_3$ pyroelectric detector array, which permitted the introduction of a corrective factor of 1.6 to the average fluence. Taking into account the uncertainty with regard to the position of the droplet inside the laser beam, the values of the fluences were given within a percentage error of about 25%. Checking of the laser pulse shape and the energy delivered for each shot was carried out by means of a photon-drag detector and a calorimeter (the shot-to-shot energy variation was about 10% and the temporal shape of the output pulse was easily reproducible). The oscillogram of a typical laser pulse is shown in Fig. 2b.

Most measurements were made using an Imacon 790 converter camera, allowing framing rates of between 10^4 and 2×10^7 frames/s with fast framing and a scanning rate of between 1 ns/mm and 1 μs/mm with streak photography. The photon-drag detector situated near the interaction area transmitted the laser signal; this, coupled with the monitor signal from the camera then indicated the framing instant, allowing perfect synchronization of the framing and the interaction. Figure 2a is an example of this type of recording in the case of a pulse of 180 J for a time of 2 μs and a framing rate of 2×10^6 frames/s.

The framing instant was thus measured to an accuracy of 10 ns for a rate of 2×10^6 frames/s and of 100 ns for a rate of 2×10^5 frames/s. The illumination of the interaction area was achieved using an argon-type ionic laser. Two helium-neon lasers helped to center the droplet. A video unit allowed the particle diameter to be checked up to the instant of the laser shot.

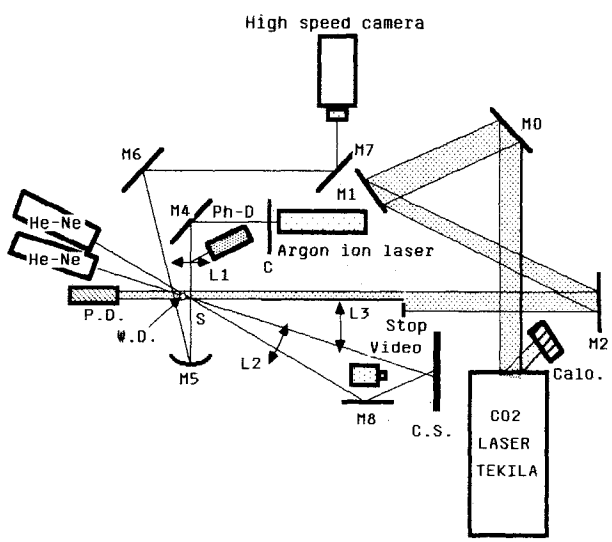

Fig. 1 Experimental apparatus (M0–M8 = plane or concave mirrors, L1–L3 = convergent lenses, P.D. = photon-drag detector, argon = laser probe, He-Ne = alignment laser, Ph-D = photodetector, Calo = calorimeter, C.S. = control screen, C = chopper; W.D. = water droplet, S = stop).

Experimental Results

High-speed photographs of the irradiated droplet history allowed us to observe the evolution of the different events that can occur sequentially. In fact, the experiments carried out enabled the vaporization of the water droplets to be revealed during the very first moments of the interaction. This mechanism preceded the deformation of the drop. This deformation was greater or lesser according to the average incident fluence and the droplet size. During this phase of deformation, ejection of liquid matter was observed from the front and then the back of the particle. The drop might then shatter according to the degree of deformation occurring.

The experiments presented in this paper were carried out in a narrow range of fluences.

Vaporization

Figure 3 shows the vaporization phase of a water droplet with an initial radius $R = 305$ μm (surface absorption case) subjected to a laser beam of average fluence 1.9 J/cm^2 (maximum local fluence ≈ 3 J/cm^2) for a total exposure time $t_p = 2$ μs. The time interval between two consecutive frames was 500 ns and the exposure time of each frame was 100 ns.

Heating of the irradiated side occurred first at a narrow thickness of the droplet ($L_{abs} = 10$ μm). When the vaporization

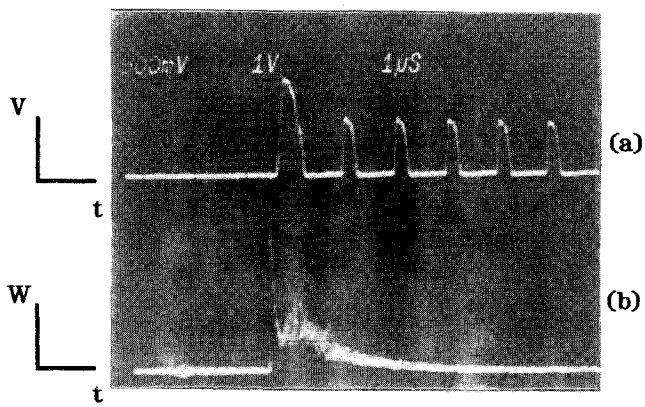

Fig. 2 Typical oscillogram recordings: a) trace of camera monitor (this signal gives the time associated with different images); b) laser pulse wave form.

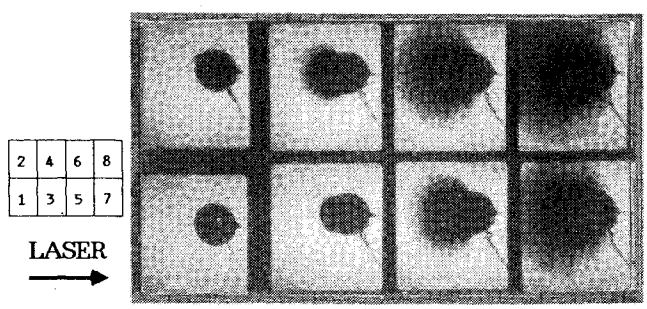

Fig. 3 High-speed photographs of the irradiated droplet history [radius = 305 μm, average fluence = 1.9 J/cm^2 (maximum local fluence 3 J/cm^2), interframe time $\Delta t = 500$ ns, the laser is incident from the left, $t_p = 2$ μs].

temperature was reached (reaction time about 1 μs), water vapor was ejected from the front side.

Under different conditions, we observed the vapor development, which was preceded by a rapidly expanding shock wave propagating in the air at a rate of about 660–750 m/s in the time interval 0–2.1 μs (the time for formation and setting in motion of the shock was estimated at 1.2–1.3 μs). The velocity then decreased to a value of 500–550 m/s in the time interval 2.1–3.1 μs.

Figures 4 and 5 present the evolution with respect to time of the axial and radial dimensions of the vapor from the initial droplet diameter. In the case of the axial dimension X_A, the drop and vapor together were measured, as opposed to the case of radial dimension Y_R, where only the vapor phase was taken into account. The liquid particle radii were between 230 and 300 μm. The average laser fluences used were 1.8–2.15/cm^2 for a pulse time of 2 μs. The moment $t = 0$ corresponded to the arrival time of the pulse at the droplet. The average intensities, constant for 1 μs, were about 1.2 and 1.4×10^6 W/cm^2.

Note that a non-negligible reaction time was necessary to heat and then begin to vaporize the water droplet. Taking into account the expansion velocity of the vapor and the shock wave preceding it, this time was estimated at 1.2–1.3 μs.

The hot vapor expanded with axial and radial velocities of about 300–350 m/s in the time interval 0–2.1 μs. These velocities then decreased to around 200 m/s in the time interval 2.1–3.1 μs. A large error could have been made concerning the vapor axial expansion velocity. In fact, the photographs do not enable the liquid/vapor interface to be observed. Experiments carried out using a flash x-ray camera could in the future allow us to follow the evolution of this interface. On the other hand, an example of streak photography of a droplet is presented in Fig. 6. This droplet (radius $R = 310$ μm) was subjected to pulses of average fluence 1.95 J/cm^2 for a total exposure time of 3.5 μs. (The average intensity was 8×10^5 W/cm^2). The scanning rate used was 2 μs/cm. It is possible to observe, on the plate, a shock wave being propagated in air during the first microsecond at a velocity of 638 m/s, preceding the vapor expansion in which there is a rarefaction fan of velocity 320 m/s. The average vapor ejection velocity during the first instants of vaporization varied between 150 and 300 m/s according to the experimental conditions.

These measurements, deduced from the framing and streak photographs, show that the shock waves created on the water droplets were proportional to t^1 during the first instants of the interaction (about 1 μs after the start of the motion of the shock wave) and were afterward proportional to $t^{0.4}$, in accordance with previously published results.[4] Figure 7 compares the experimental results with the theoretical expansion of a spherical blast wave described by Sedov.[17]

The law of motion and the velocity of the shock wave in spherical symmetry can be expressed by

$$r = (E/\rho)^{1/5} t^{2/5} \tag{1}$$

$$v = 2/5(E/\rho)^{1/5} t^{-3/5} \tag{2}$$

This model is obviously not applicable to the beginning of the interaction. In fact, when the shock wave started moving, the laser pulse was not completed. A certain amount of energy continued to reach the droplet. This could explain the evolution being proportional to t^1 during this sustained phase. The transition between the sustained and nonsustained phases of the flow was situated at around 1.5 μs (i.e., about 2.7 μs after the beginning of irradiation).

By equating the laser energy absorbed with the laser energy necessary to totally vaporize a water droplet of radius R, we obtain the approximation,

$$\frac{4/3\pi R^3 \rho (C_p \Delta T + l_v)}{\pi R^2 Q_A(R)} \tag{3}$$

For large droplets: $Q_A \approx 1$ and $F = 4/3\rho \cdot L_v \cdot R$ (4)

For small droplets: $Q_A \approx R/L_{abs}$ and $F = 4/3\rho \cdot L_v \cdot L_{abs}$ (5)

where F is in units of J/cm^2.

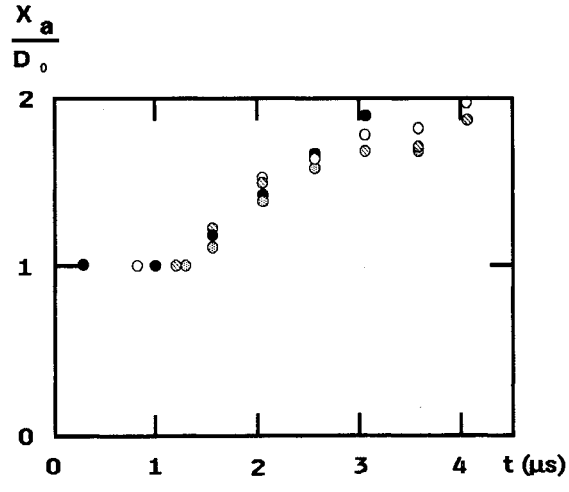

Fig. 4 Axial evolution of the vapor as a function of time [X_A = axial dimension of the optically dense phase (liquid + dense vapor), D_0 = initial diameter of the droplet ($460 < D_0 < 600$ μm), $t = 0$, arrival time of the laser pulse at the droplet, average fluence = 1.8–2.1 J/cm^2 (maximum value 1.9–3.3 J/cm^2), average intensity = $1.2–1.4 \times 10^6$ W/cm^2, laser pulse duration on order of 2 μs].

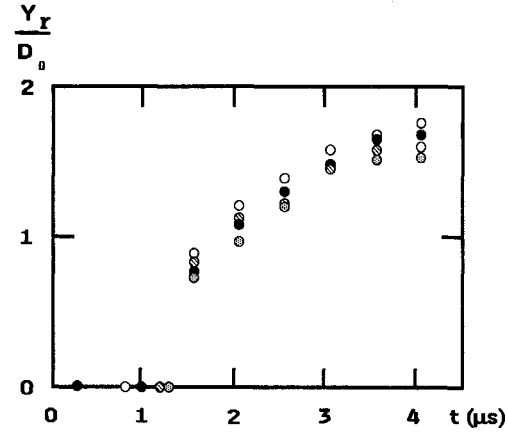

Fig. 5 Radial evolution of the vapor as a function of time [Y_R = radial dimension of the optically dense phase (dense vapor), D_0 = initial diameter of the droplet ($460 < D_0 < 600$ μm), average fluence = 1.8–2.1 J/cm^2, average intensity = $1.2–1.4 \times 10^6$ W/cm^2, laser pulse duration on order of 2 μs].

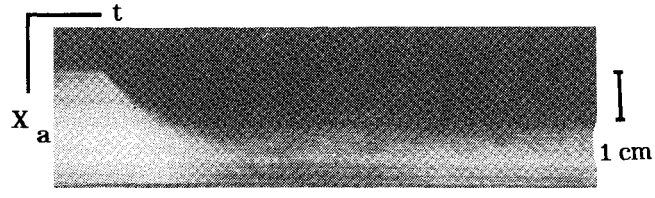

Fig. 6 Streak photography of an irradiated droplet, 2 μs/cm [radius = 310 μm, average fluence = 1.95 J/cm^2 (maximum value 3.1 J/cm^2), average intensity = 8×10^5 W/cm^2]. Note a shock wave preceding the vapor and rarefaction waves.

Thus, we can very roughly estimate that an exposure on the order of 7 J/cm^2 is necessary to totally vaporize a water droplet of radius $R = 20\ \mu$m, whereas 100 J/cm^2 is necessary with a particle of radius $R = 300\ \mu$m. These fluences are much greater than those used in our experiments. But we were dealing only with a surface absorption process—heating did not occur throughout the drop, but rather in only a very thin liquid layer ($L_{abs} = 10\ \mu$m). Vaporization effects, deformation, and shattering were thus observed for much weaker fluences ($F \approx 2$ J/cm^2). For our experimental conditions using a pulse laser (large drops), it thus seems that the mechanism of shattering was more significant than that of total vaporization.

On the other hand, Fig. 8 shows the total vaporization of a particle of radius 8 μm (volume absorption process) when exposed to an average fluence of 2.5 J/cm^2 (maximum local fluence 4 J/cm^2). This value is slightly lower than the necessary fluence $F \approx 3.5$ J/cm^2 obtained by Eq. (5), taking into account the coefficient of the absorption ($Q_A \approx 0.8$). This is explained by an underestimation of the average fluence value at the particle.

A more detailed description can be obtained using Knight's convective vaporization model[18] for droplets of sufficiently large radius compared to the radiation absorption length ($L_{abs} = 10\ \mu$m) and for sufficient laser intensities ($> 10^4$ W/cm^2), which was the case in our experiments. Knight's model uses a Knudsen layer at the liquid/vapor interface, thus treating the part of the flow outside the local thermodynamic equilibrium as a discontinuity. Beyond this discontinuity, the flow is described by a classical method (i.e., "the characteristic treatment"). The diagrams in Fig. 9 represent the main flow areas deduced from this model in the form of graphs X–Y and R–t.

Deformation

Figure 10 shows a water particle of radius $R = 126\ \mu$m exposed to a laser pulse of average fluence $F = 2.6$ J/cm^2 for a total pulse time of 3.5 μs. The interframe time was 5 μs and the exposure time 1 μs. After the vaporization phase, which can still be observed in frame 2, the droplet became deformed, decreasing in diameter along the laser beam axis and lengthening along the perpendicular axis. Two dimensionless numbers were defined as characterizing the shape change:

$$R = R_0/R_1 \quad \text{and} \quad L = L_0/L_1$$

where R_1 is the radius of curvature of the irradiated face of the droplet, R_0 the radius of curvature of the face not irradiated, L_0 the dimension of the droplet along the beam axis, and L_1 the dimension of the droplet along the perpendicular axis.

Figure 11 shows the sign conventions adopted for the measurement of the radius of curvature. Figure 12 shows the evolution of parameter L with time for different experimental conditions. Generally, the curves decrease until reaching a plateau value, the decrease being essentially linked to the increase in parameter L_1. For similar laser parameters, the values of L with time were all smaller because the initial droplet radius was small. For similar initial droplet radii, L was smaller because the average laser fluence was high.

Figure 13 presents the evolution with respect to time of parameter R for the same experimental conditions as those presented in Fig. 12. The different curves decrease until reaching a minimum value and then increase. Note that this minimum value is a descending function of the initial droplet radius and an ascending function of the laser fluence brought into play. The liquid particle deformation can be explained by the effective overpressure P_e caused by the rapid vapor flow from the irradiated surface. The characteristic deformation times were relatively large compared to the laser pulse time, in such a way that the effective overpressure could be considered to be

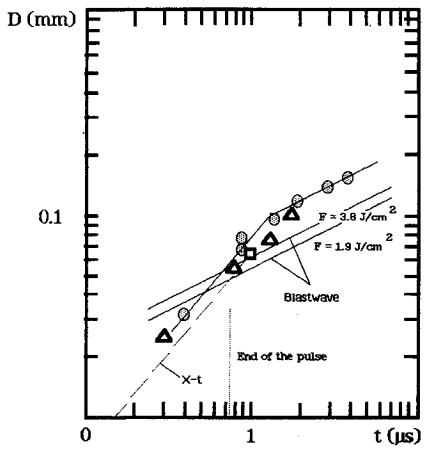

Fig. 7 Development of shock wave created on a water droplet. Experimental results: ○, △ deduced from instantaneous photographs, □- - - deduced from recordings X–t, —— development of a spherical blast wave with energy absorbed 1.9–3.8 J/cm^2.

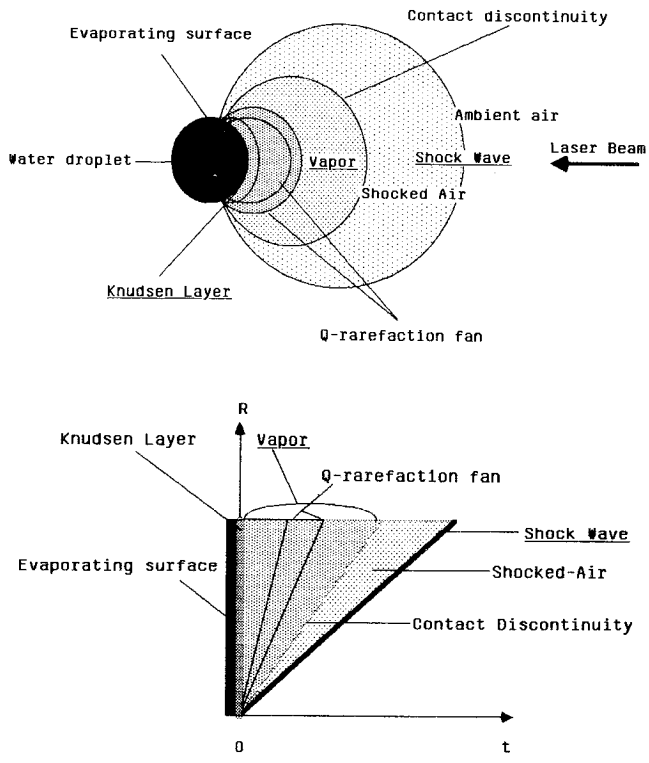

Fig. 8 Interaction with smaller nonsuspended droplets [radius = 8–30 μm, average fluence = 2.5 J/cm^2 (maximum value 4 J/cm^2), interframe time = 5 μs, laser incident from the right].

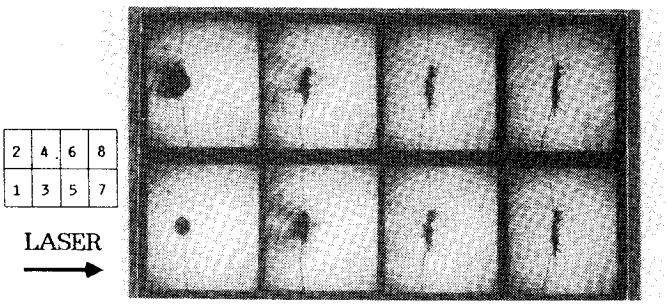

Fig. 9 Droplet vaporization schematic model.

created instantaneously at the drop surface. A model described by Singh and Knight[15] could thus be applied to our experimental case. This model uses a mechanical impulse I per unit surface delivered to the drop, defined by the momentum conservation equation

$$4/3\pi R^3 \rho U = 2\pi R^2 I \tag{6}$$

The mechanical impulse I can be expressed as a function of the average effective overpressure P_e as

$$I = \bar{P}_e \cdot t_p \tag{7}$$

Hypothesizing a cosinal distribution of the vapor pressure around the drop, we get

$$\bar{P}_e = P_{e\max}/3 \tag{8}$$

On the other hand, supposing that the vapor flow is sonic at the liquid/vapor interface, it is possible to evaluate P_e as a function of incident laser intensity using the approximation,

$$\frac{P_e}{\phi} \approx \frac{\gamma+1}{\gamma}\frac{m \cdot c}{m \cdot L_v} \approx 24 \times 10^{-5} \quad (\mathrm{N/cm^2})/(\mathrm{W/cm^2}) \tag{9}$$

from which the mechanical impulse is written as

$$I = 8 \times 10^{-5}\phi \cdot t_p = 8 \times 10^{-5} \cdot F \quad \mathrm{N \cdot s/cm^2} \tag{10}$$

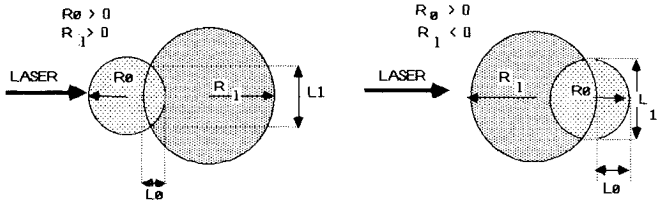

Fig. 10 High-speed photographs of the irradiated droplet history [radius = 126 μm, average fluence = 2.6 J/cm^2 (maximum value 4.1 J/cm^2), interframe time $\Delta t = 5$ μs, laser incident from the left ($t_p = 3.5$ μs)].

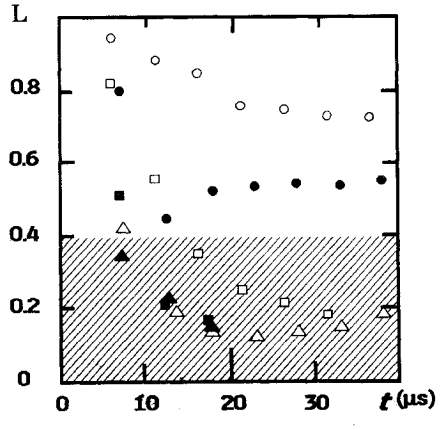

	Fluence, J/cm^2	Initial radius, μm		Fluence, J/cm^2	Initial radius, μm
●	2.15	220	○	1.70	130
■	2.10	65	□	2.60	126
▲	2.10	35	△	2.97	140

Fig. 11 Sign conventions adopted for the measurement of the radius of curvature.

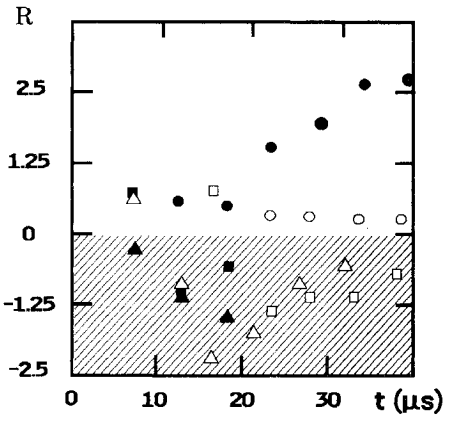

Fig. 12 Evolution with time of the parameter L (no deformation was observed on a drop of 130 μs irradiated with a fluence of 1.45 J/cm^2).

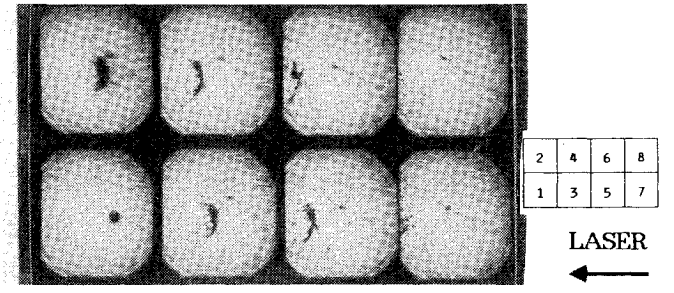

Fig. 13 Evolution with time of the parameter R (same experimental conditions as those presented in Fig. 11).

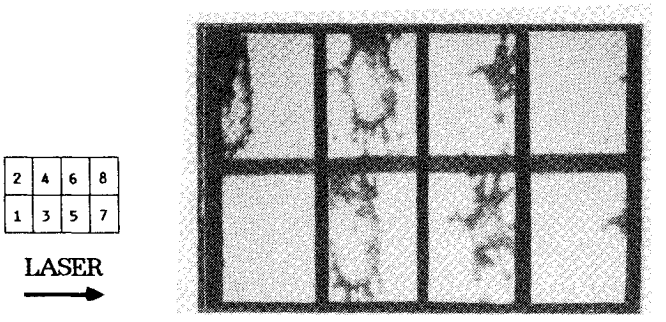

Fig. 14 Shattering of a water droplet [radius = 35 μm, average fluence = 2.1 J/cm^2 (maximum value 3.3 J/cm^2), $\Delta t = 5$ μs, laser incident from the right].

The characteristic forces acting on the fluid inside the drop can be expressed as a function of I and of R,

$$\text{Inertia} = \rho(I/\rho R)^2 = I^2/\rho \tag{11}$$

$$\text{Surface tension} = \sigma R \tag{12}$$

$$\text{Viscous force} = \gamma\rho(I/\rho R^2)r^2 = Iv \tag{13}$$

The deformation phenomenon is essentially linked to the ratio of surface tension and inertia $\rho\sigma R/I^2$.

Shattering

During the deformation phase of the droplet (Fig. 10), projections of liquid matter from the droplet surface were observed. For numerous test conditions, we noted that these projections of matter usually took place on the radiated side of the droplet and reached the opposite side after a time lag of between 5 and 15 μs. The flow from the irradiated surface can be explained by the intense heating that boils the water. Sup-

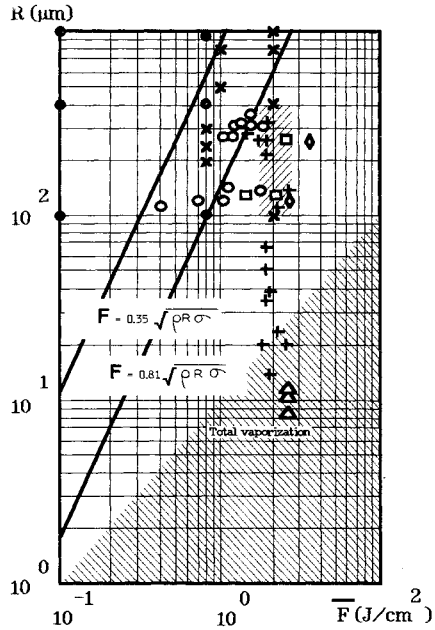

Result	Institut de Mecanique des Fluides de Marseilles	Avco
Shattering		
$t_p = 2\ \mu s$	+	
$t_p = 3.5\ \mu s$	□ ////	X
$t_p = 5\ \mu s$	◇	
No shattering	○	●
Total vaporization	▽	

Fig. 15 High-speed photographs of the irradiated droplet [radius = 400 μm, average fluence = 2.45 J/cm² (maximum value 3.9 J/cm²), interframe time Δt = 100 μs].

posing that the flow from the surface not directly irradiated has the same origin, the measured time lags correspond to the propagation velocity across the drop, which was 20–25 m/s. This velocity corresponds to a hydrodynamic convection flow carrying vapor bubbles created by the boiling toward the nonexposed surface. More recent results[19] (comparisons of computed temperature contours to explosive vaporization patterns) show that this ejection of material from the back surface can be explained by the explosive vaporization from hot spots caused by electromagnetic heating by the laser pulse (and not caused by shock wave propagation through the droplet).

For example, we were able to measure, on recordings of X, t for a drop of 200 μm radius irradiated with an average fluence of 2.4 J/cm², ejection of small water droplets 5–10 μs after the start of vaporization. An ejection velocity of 30 m/s for these fragments was measured.

The phase just described does not really constitute a shattering phase that can be considered to be the total shattering of the particle (Figs. 14 and 15). Figure 14 shows the shattering of a droplet of radius $R = 35\ \mu m$ subjected to a laser fluence $F = 2.1$ J/cm². The interframe time was 5 μs and the exposure time 1 μs. The first frame was taken at time $t = 1.6\ \mu s$ after the arrival of the pulse at the drop. The shattering time (frame 6) could be estimated as 25 μs after the start of the interaction.

Figure 14 shows the shattering of a drop of radius $R = 400\ \mu m$ ($t = 550\ \mu s$, frame 5) exposed to laser fluence $F = 2.45$ J/cm². The interframe time was 100 μs and the exposure time 20 μs. The first frame was taken at time $t = 150\ \mu s$ after the start of the pulse. Note that the shattering time is an ascending function of the initial droplet radius and a descending function of the laser fluence.

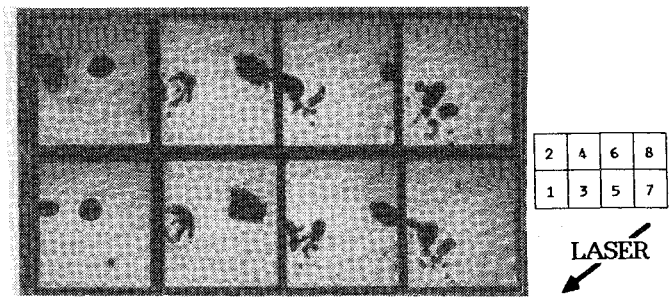

Fig. 16 Shattering limit as a function of the average fluence [—— criteria of theoretical shattering given by Singh (Avco), //// region dominated by forces of viscosity].

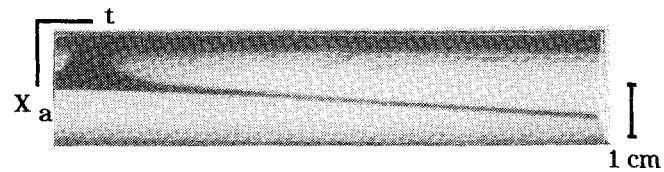

Fig. 17 Streak photography of the irradiated droplet [streak = 10 μs/cm, radius = 138 μm, average fluence = 2.25 J/cm² (maximum value 3.6 J/cm²), opening of camera 0.2 μs after laser pulse arrival at drop].

Moreover, according to Figs. 11 and 12, the shattering was directly linked to the amount of deformation suffered by the drop. The values $L = 0.4$ and $R = 0$ effectively separate all of the deformation curves into two groups: 1) those resulting in total droplet shattering (a time existing such that $L < 0.4$ and $R < 0$) and 2) those deforming without shattering (for all times t, we get $L > 0.4$ and $R > 0$).

Figure 16 presents the different shattering experimental results obtained in a fluence-radius graph. A shattering threshold fluence (average value) can thus be determined to be situated around 1.7 J/cm² in our experiments on particles of radii greater than 100 μm. Shattering thresholds have also been proposed by different authors. A different criterion linked to the product of overpressure p_e and pulse length t_p has been proposed. Below a minimum value of $(p_e \cdot t_p)$, the drops can be vaporized on the surface and then deformed. But they do not shatter. Above this value, drop deformation always precedes their shattering into satellite drops.

This shattering will take place if the specific impulse delivered to the droplet exceeds 10–20 dyne · s/cm² for Singh and Knight[15] (average fluence 0.8–2.5 J/cm²), 30 dyne · s/cm² for Kafalas and Ferdinand[13] and Kafalas and Herrmann,[14] 2.7 J/cm² for Pistoresi,[20] and 1.7 J/cm² or 14 dyne · s/cm² (maximum value 2.7 J/cm² or 22 dyne · s/cm²) for drops of radii greater than or equal to 100 μm for the experiments presented in this paper. See Fig. 8. These results are all in relatively good agreement for quite broad experimental conditions (a factor of 1 : 3 maximum). Study of the ejected fragments is very complex. For example, for a drop of 400 μm radius, fragments of 7–12 μm radii have been observed. Be that as it may, the fragment dimensions obtained can be evaluated and compared with the equation[15]

$$R_f \approx R_0/(1 + 0.205I^2/\rho R_0\sigma) \qquad (14)$$

Propulsion

Figure 17 is a photograph of the interaction taken in X–t; the scanning rate was 10 μs/cm. The droplet radius was $R = 138\ \mu m$ and the laser fluence $F = 2.25$ J/cm². In addition to the vaporization phase on the side facing the laser beam, we observed a movement of the droplet. The propulsion velocity in the case in Fig. 17 was estimated at 7.4 m/s. On this streak

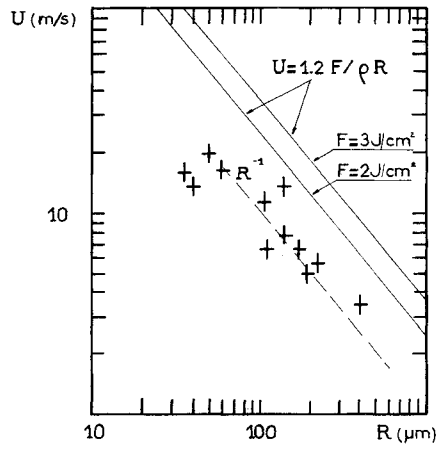

Fig. 18 Ejection velocity of drops under effect of radiation as a function of radius. Comparison with the expression $U = 1.2F/\rho R$ with an average fluence of 2–3 J/cm² corresponding to the results presented.

photograph, note the water vapor coming from the vaporization of the drop about 1.2 μs after the laser pulse arrival. This vapor developed in about 6 μs. The ejection of matter can very clearly be seen almost simultaneously from the front and back faces of the drop, about to 8 μs after irradiation at an average velocity of about 20 m/s ($\Delta t = 40$ μs).

In addition to the vaporization phase on the side facing the laser beam, we observed a movement of the droplet. Different experimental results obtained are shown in Fig. 18 for particles of 35–400 μm radii irradiated with an average fluence of 2.1–3 J/cm². These results give the evolution αR^{-1} and an order of magnitude for the propulsion velocity; however, they may have been altered by the presence of the silk thread supporting the drop.

We have, on the other hand, calculated the center of mass velocity U obtained from Eq. (6) as

$$U = 2\pi R^2 \cdot I/(4/3\pi R^3 \rho) \qquad (15)$$

We can establish that the measured values of the ejection velocity of the drops was systematically lower than the calculated values using the approximation above.

Other Mechanisms

Other mechanisms that can greatly influence the laser beam propagation in the atmosphere were also observed. These were:

1) The coalescence mechanism of the ejected fragments. For example, fragments of 5–7 μm radii able to coalesce 10–15 μs after the start of shattering of a drop of 22 μs radius.

2) A shade effect of large drops on small ones. For example, a drop of 13 μm radius was completely protected from laser radiation by another particle ($R = 18$ μm) at a distance of 20 μm. The latter was vaporized, strongly deformed, and then shattered 20 μs after the start of irradiation ($F = 2.5$ J/cm²).

3) Recondensation. We have not been able to observe this in a very clear way, but it exists and plays a devastating role.

Conclusion

Knowledge of the thermomechanical mechanisms occurring when a laser beam interacts with a water droplet is important in order to maximize the progagation of high-intensity laser pulses, especially for atmospheric conditions such as haze, fog, or clouds where airborne particle concentrations are high and for rain where water drops are large. Experiments have been conducted to identify the main mechanisms that can occur sequentially throughout laser interaction without defining precisely which ones, in the experimental conditions studied, dominate with respect to the others. Other experiments are being planned over a wider range of fluences. In order to learn more detail concerning the limits of total droplet vaporization, other experiments on nonsuspended small particles ($R \leq 10$ μm) are in preparation. The recondensation phenomenon undoubtedly has a great influence on the limitation of the effect of laser clearing. A more detailed study of these phenomena is envisaged. Finally, complete modeling of the different mechanisms described in this paper has been undertaken.

Acknowledgments

The authors would like to thank J. P. Fragassi and E. Mazoyer-Carrer for their assistance throughout the course of the experiments. Thanks are also extended to Dr. G. Inglesakis for helpful discussions. This work is supported by the Direction des Recherches, Etudes et Techniques under Contract 83-334 and 85-028.

References

[1]Lencioni, D. E., "The Effects of Dust in 10.6 μm Laser Induced Air Breakdown," *Applied Physics Letters*, Vol. 23, July 1973, pp. 12–14.

[2]Smith, D. C. and Brown, R. T., "Aerosol-Induced Air Breakdown with CO_2 Laser Radiation," *Journal of Applied Physics*, Vol. 46, March 1975, pp. 1146–1154.

[3]Reilly, J. P., Singh, P., and Weyl, G., "Multiple Pulse Laser Propagation Through Atmosphere Dusts at 10.6 Microns," AIAA Paper 77-697, June 1977.

[4]Reilly, J. P., Singh, P., and Glickler, S., "Laser Interaction Phenomenologie for Water Aerosols at CO_2 Wavelengths," AIAA Paper 77-659, June 1977.

[5]Autric, M., Caressa, J. P., Bournot, Ph., Dufresne, D., and Sarazin, M., "Propagation of Pulsed Laser Energy Through the Atmosphere," *AIAA Journal*, Vol. 19, Nov. 1981, pp. 1415–1421.

[6]Amimoto, S. T., Whittier, J. S., Ronkowski, F. G., Valenzuela, P. R., Harper, G. N., and Hofland, R. J., "DF Laser Pulse Breakdown Induced by Maritime Aerosols," *AIAA Journal*, Vol. 22, Aug. 1984, pp. 1108–1114.

[7]Mullaney, G. J., Christiansen, W. H., and Russel, D. A., "Fog Dissipation using a CO_2 Laser," *Applied Physics Letters*, Vol. 13, Aug. 1968, pp. 145–147.

[8]Sutton, G. W., "Fog Dispersal by High Power Lasers," *AIAA Journal*, Vol. 8, Oct. 1970, pp. 1907–1910.

[9]Lencioni, D. E. and Lowder, J. E., "Aerosol Clearing with a 10.6 μm Precursor Pulse," *IEEE Journal of Quantum Electronics*, Vol. QE10, Feb. 1974, pp. 235–238.

[10]Sutton, G. W., "Fog Hole Boring with Pulsed High-Energy Laser: An Exact Solution Including Scattering and Absorption," *Applied Optics*, Vol. 17, No. 21, Nov. 1978, pp. 3424–3430.

[11]Autric, M., Caressa, J.-P., Dufresne, D., and Bournot, Ph., "Atmospheric Propagation of Two CO_2 Laser Pulses," *AIAA Journal*, Vol. 22, Jan. 1984, pp. 75–80.

[12]Autric, M., Dufresne, D., Caressa, J. P., Vigliano, P., Carrer, E., and Chhim, V., "Aerosol Clearing Using a High Power CO_2 Laser Pulse," *Proceedings of the 5th International Symposium on Gas Flow and Chemical Lasers*, Institute of Physics Conference Series No. 72, Adam Higler Ltd., Boston, 1985, pp. 385–390.

[13]Kafalas, P. and Ferdinand, A. P. Jr., "Fog Droplet Vaporization and Fragmentation by a 10.6 μm Laser Pulse," *Applied Optics*, Vol. 12, Jan. 1973, pp. 29–33.

[14]Kafalas, P. and Herrmann, J., "Dynamics and Energetics of the Explosive Vaporization of Fog Droplets by a 10.6 μm Pulse," *Applied Optics*, Vol. 12, April 1973, pp. 772–775.

[15]Singh, P. I. and Knight, C. J., "Pulsed Laser-Induced Shattering of Water Drops," *AIAA Journal*, Vol. 18, Jan. 1980, pp. 96–100.

[16]Cloupeau, M., Laboratoire d'Aérothermique du CNRS, Meudon, France.

[17]Sedov, L., *Similitude et Dimensions en Mécanique*, Editions MIR, Moscow, 1977, pp. 232–277.

[18]Knight, C. J., "Theoretical Modeling of Rapid Surface Vaporization with Back-Pressure," *AIAA Journal*, Vol. 17, May 1979, pp. 519–523.

[19]Pendleton, J. D., "Water Droplet Irradiated by a Pulsed CO_2 Laser: Comparison of Computed Temperature Contours with Explosive Vaporization Patterns," *Applied Optics*, Vol. 24, June 1985, pp. 1631–1637.

[20]Pistoresi, D. J., "Comparison of Pulsed D.F. and CO_2 Laser Propagation Through Fog and Rain," AIAA Paper 81-1252, June 1981.